1 **Low dose AKT inhibitor miransertib cures PI3K-related vascular**

2 **malformations in preclinical models of human disease**

3

4 Piotr Kobialka[1,¥], Helena Sabata[1,¥], Odena Vilalta[1], Ana Angulo-Urarte[1], Laia Muixí[1], Jasmina

5 Zanoncello[1], Oscar Muñoz-Aznar[2], Nagore G. Olaciregui[3], Cinzia Lavarino[3], Veronica Celis[2],

6 Carlota Rovira[4], Susana López[5], Eulàlia Baselga[6], Jaume Mora[2,7], Sandra D. Castillo[1,ϒ,*], Mariona

7 Graupera[1,8,ϒ,*]

8

9 [1]Endothelial Pathobiology and Microenvironment, Josep Carreras Leukaemia Research Institute,

10 08916, Barcelona, Spain.

11 [2]Pediatric Cancer Center Barcelona, Hospital Sant Joan de Déu Barcelona, 08950, Barcelona,

12 Spain.

13 [3]Laboratory of Molecular Oncology, Hospital Sant Joan de Déu, 08950, Barcelona, Spain.

14 [4]Department of Pathology. Hospital Sant Joan de Déu Barcelona, 08950, Barcelona, Spain.

15 [5]Vascular Surgery, Hospital de la Santa Creu i de Sant Pau, 08041, Barcelona, Spain.

16 [6]Department of Dermatology, Hospital Sant Joan de Déu, 08950, Barcelona, Spain.

17 [7]Developmental Tumor Biology Laboratory, Institut de Recerca Sant Joan de Déu, 08950,

18 Barcelona, Spain.

19 [8]CIBERONC, Instituto de Salud Carlos III, Madrid, Spain.

20 [¥]Joint first authors

21 [ϒ]Joint last authors

22 **To whom correspondence should be addressed: S.D.C. (scastillo@carrerasresearch.org) and

23 M.G. (mgraupera@carrerasresearch.org) Tel: +34 93 557 2800

24   **ABSTRACT**

25   Low-flow vascular malformations are congenital overgrowths composed by abnormal blood

26   vessels potentially causing pain, bleeding, and obstruction of different organs. These diseases

27   are caused by oncogenic mutations in the endothelium which result in overactivation of the

28   PI3K/AKT pathway. Lack of robust *in vivo* preclinical data has prevented the development and

29   translation into clinical trials of specific molecular therapies for these diseases. Here, we describe

30   a new reproducible preclinical *in vivo* model of PI3K-driven vascular malformations using the

31   postnatal mouse retina. This model reproduces human disease with *Pik3ca* activating mutations

32   expressed in a mosaic pattern and vascular malformations formed in veins and capillaries. We

33   show that active angiogenesis is required for the pathogenesis of vascular malformations caused

34   by activating *Pik3ca* mutations. Using this model, we demonstrate that low doses of the AKT

35   inhibitor miransertib both prevents and induces the regression of PI3K-driven vascular

36   malformations. We confirmed miransertib efficacy in isolated human endothelial cells with

37   genotypes spanning most of human low-flow vascular malformations.

38

39   **Keywords**

40   AKT/ PI3K / Endothelial cell / Vascular malformations / Angiogenesis

41

42   **Short title**

43   Miransentib regresses PI3K-related vascular malformations

Introduction

44

45   Vascular malformations are a congenital group of diseases composed of abnormal vascular

46   channels that can occur anywhere in the body and potentially had a major impact on the quality

47   of life of patients. They tend to be painful and disfiguring, and many leading to bleeding, recurrent

48   infections, thrombosis, organ dysfunction, and even death (Van Damme *et al*, 2020). Vascular

49   malformations can be classified as low-flow (venous, lymphatic and capillary) and fast-flow

50   (arteriovenous) lesions, the former being the most frequent subtype. Vascular malformations

51   appear during embryonic development, when vascular growth factors are produced at high levels,

52   and expand proportionally with the physiological growth of the patient (Pang *et al*, 2020). Of note,

53   vascular malformations may occur in isolation or as a part of a syndrome (Canaud *et al*, 2021).

54   At present, there is no molecularly targeted therapy in the current management for these

55   diseases. Instead, standard of care includes a broad spectra of mostly inefficient and invasive

56   techniques including bandage compression, surgical excision, and sclerosing approaches

57   (Castillo *et al*, 2019).

58   Overactivation of phosphoinositide 3-kinase (PI3K) signalling is a hallmark of most low-flow

59   vascular malformations (Castillo *et al*, 2019; Mäkinen *et al*, 2021; Canaud *et al*, 2021). Sporadic

60   venous malformations, the most common type of vascular malformations, are caused by gain-of-

61   function mutations either in the endothelial tyrosine kinase receptor TEK/TIE2 or in the PI3K

62   catalytic subunit alpha *PIK3CA* (Limaye *et al*, 2015; Castillo *et al*, 2016a; Castel *et al*, 2016); with

63   *TEK* and *PIK3CA* mutations being mutually exclusive. Also, 80% of lymphatic malformations are

64   caused by activating *PIK3CA* mutations (Boscolo *et al*, 2015; Luks *et al*, 2015; Mäkinen *et al*,

65   2021). In addition, venous, lymphatic and/or capillary malformations are frequently present in

66   overgrowth syndromes caused by *PIK3CA* mutations, the so-called PROS (PIK3CA-related

67   overgrowth spectrum) (Keppler-Noreuil *et al*, 2015). *PIK3CA* mutations in vascular malformations

68   are similar to those found in epithelial cancer, being the missense mutations in the helical

69   ($PIK3CA^{E542K}$, $PIK3CA^{E545K}$) and the kinase ($PIK3CA^{H1047R}$) domains the most prevalent (Samuels

70   *et al*, 2004).

3

71   *PIK3CA* encodes the p110α lipid kinase protein, which is a major signalling component

72   downstream of growth factor receptor tyrosine kinases (RTKs) (Bilanges *et al*, 2019; Kobialka &

73   Graupera, 2019). Specifically in endothelial cells, p110α is activated by the vascular endothelial

74   growth factor receptors (VEGF-R) and TIE tyrosine kinase receptors (Graupera & Potente, 2013).

75   Hence, it is not surprising that p110α is the sole class I PI3K isoform required for blood and

76   lymphatic vascular development (Graupera *et al*, 2008; Stanczuk *et al*, 2015). p110α catalyses

77   the phosphorylation of the lipid second messenger phosphatidylinositol-4,5-triphosphate (PIP$_2$) to

78   phosphatidylinositol-3,4,5-triphosphate (PIP$_3$) at the cell membrane (Bilanges *et al*, 2019). PIP$_3$,

79   in turn, contributes to the recruitment and activation of a wide range of downstream targets, the

80   serine-threonine protein kinase AKT (also known as protein kinase B, PKB) being critical in this

81   cascade. The PI3K-AKT signalling pathway regulates many cellular processes that are key for

82   endothelial cell biology, including cell proliferation, survival, and motility (Bilanges *et al*, 2019;

83   Manning & Toker, 2017). There are three isoforms of AKT (AKT1, 2 and 3), showing high

84   homology but being not redundant. AKT1 and AKT2 are broadly expressed, with AKT1 being the

85   predominant isoform in endothelial cells (Chen *et al*, 2005; Ackah *et al*, 2005). *PIK3CA* and *TEK*

86   gain-of-function mutations in endothelial cells lead to AKT hyper-phosphorylation which result in

87   enhanced endothelial cell proliferation and resistance to cell death induced by growth factor

88   withdrawal (Cai *et al*, 2019; Le Cras *et al*, 2020). Of note, pathological proliferation burst of

89   cultured *PIK3CA* and *TEK* mutant cells is elicited by supplementation with external growth factor

90   signals.

91   The discovery that most low-flow lesions are caused by overactivation of PI3K signalling has

92   catalysed the repurpose of PI3K pathway inhibitors for these diseases. Given that pathological

93   endothelial mutant cells primarily depend on AKT signalling, inhibition of AKT is a promising

94   strategy for low-flow vascular malformations. Amongst AKT inhibitors, miransertib (ARQ 092, MK-

95   7075) is a potent and selective allosteric AKT inhibitor showing higher specificity for the AKT1

96   isoform. Miransertib suppresses AKT activity by inhibiting membrane-bound active form of AKT

97   and preventing activation of the inactive form of AKT (Yu *et al*, 2015). This inhibitor has shown

98   efficacy in preclinical studies for PI3K-driven tumours (Yu *et al*, 2015, 2017) and Proteus

99 syndrome (Lindhurst *et al*, 2015), which is caused by a somatic AKT gain-of-function mutation.

100 Also, compassionate use of this inhibitor has shown therapeutic efficacy in patients with Proteus

101 and PROS (Leoni *et al*, 2019; Biesecker *et al*, 2020; Forde *et al*, 2021).

102 Here, we show that active angiogenesis is required for the formation of *Pik3ca*-driven vascular

103 malformations and report a unique *in vivo* model of PI3K-driven vascular malformations that

104 allows a more accurate understanding of the dynamic pathogenesis of these diseases and thus

105 a more efficient assessment of therapeutic strategies. In addition, we show how analysing patient-

106 derived endothelial cells from vascular malformations allows for personalised medicine testing in

107 these diseases. Using a spectra of preclinical models we demonstrate the efficacy of the AKT

108 inhibitor miransertib at low dose for PI3K-driven vascular malformations both for prevention and

109 treatment strategies. Furthermore, we show that endothelial cells from *TEK* and *PIK3CA*-mutant

110 vascular malformations respond similarly to miransertib.

Results

111

112   ***Active angiogenesis is required for the formation of PI3K-driven vascular malformations***

113   Because vascular malformations appear during embryonic development when endothelial

114   mitogenic signals are produced at high concentration, we postulated that the genesis of these

115   lesions depends on the stage of vascular development. To test this idea, we took advantge of the

116   mouse retinal vasculature which allows the study of the different phases of angiogenesis. We

117   chose three developmental stages (early, intermediate and late) in which endothelial cells (ECs)

118   exhibit different dependency to mitogenic signals (Ehling *et al*, 2013). We induced the

119   endogenous expression of the *Pik3ca*^{H1047R} mutation (Kinross *et al*, 2012) in heterozygosis by

120   using the Pdgfb-iCreER mice, which expresses a tamoxifen-inducible Cre recombinase

121   specifically in ECs (Claxton *et al*, 2008). 4-Hydroxytamoxifen (4-OHT) was administered at

122   postnatal day (P)1, P7 or P15 and retinas were isolated one week later (Fig 1A). By analysing the

123   extent of vascular overgrowth, we found that both early and intermediate stages showed full

124   penetrance, with all retinas analysed developing vascular malformations (Fig 1B,C). However,

125   the degree of enhanced vascularity was more prominent and generalized in the early

126   develomnetal stage than in the intermediate period (Fig 1B-D). In contrast, only one third of the

127   retinas showed malformed vascular areas when *Pik3ca*^{H1047R} mutation was expressed at P15 (Fig

128   1B-D). By taking advantage of ROSA^{mTmG};Pdgfb-iCreER (later referred to as EC-mTmG) reporter

129   mice (Muzumdar *et al*, 2007), which expresses cell membrane-localized EGFP following Cre

130   recombination, we demonstrated that the Pdgfb-iCreER line is similarly active at all time points

131   tested (Fig 1E, F). Thus, penetrance and severity of vascular malformations in our model are

132   independent of the number of ECs recombined at the different stages. These results indicate that

133   the expression of mutant *Pik3ca* in ECs is not sufficient for the acquisition of a malformed vascular

134   phenotype and that active angiogenesis is required for PI3K-driven vascular malformations to

135   occur.

A new preclinical model of PI3K-driven vascular malformations

136

137   Our data show that expression of *Pik3ca*[H1047R] in ECs at an early stage of postnatal

138   angiogenesis leads to generalised vascular malformations. However, sporadic vascular

139   malformations appear as a mosaic disease, where malformed vascular lesions tend to be isolated

140   and focal. Hence, to better reproduce the etiology of human disease, we studied the impact of a

141   decreasing range of 4-OHT doses during early developmental stage in EC-*Pik3ca*[WT/H1047R] mouse

142   retinas (Fig 2A). To validate mosaicism and identify targeted ECs in our dosing strategy, we

143   treated EC-mTmG P1 mice in parallel with the same doses (Fig 2B, C). This approach allowed

144   us to identify the lowest 4-OHT dose (0.125 mg/kg) that led to distinguishable vascular

145   malformations with a total vascular density significantly increased compared to wild type

146   counterparts (Fig 2A, D). Also, we noticed that low dose of 4-OHT allowed the targeting of ECs

147   of all vessel subtypes including arteries, veins, and capillaries (Fig 2B). Instead, expression of

148   *Pik3ca*[H1047R] upon low dose of 4-OHT resulted in the formation of vascular malformations only in

149   veins and capillaries (Fig 3A). This is consistent with the observation that, within the blood vessel

150   compartment, *PIK3CA* mutations are only present in human venous and capillary malformations

151   (Keppler-Noreuil *et al*, 2015; Castillo *et al*, 2016a). *Pik3ca*[H1047R]-vascular malformations in

152   postnatal retinas showed enriched phospho (p)-S6 (Ser235/236) levels, a read-out for

153   PI3K/AKT/mTORC1 signalling, compared to the surrounding normal vasculature and wild type

154   retinas (Fig 3B, D). This focal PI3K signalling activation resulted in EC hyperproliferation (Fig 3C,

155   E) and accumulation of ECs, causing the overall enhanced vascularity (Fig 3C, F, G). These

156   lesions also exhibited loss of pericyte coverage, assessed by immunostaining for pericyte-specific

157   marker NG2, in contrast to non-malformed vasculature in the same retina and the control (Fig

158   EV3). Collectively, these results show that EC-specific mosaic induction of endogenous

159   *Pik3ca*[H1047R] expression during active vascular growth faithfully models human low-flow vascular

160   malformations.

161 ***Low dose AKT inhibitor miransertib prevents the formation of PI3K-driven vascular***

162 ***malformations***

163   Targeting AKT, the main player of PI3K-driven signalling in ECs, has not yet been assessed

164 *in vivo* in vascular malformations. Thus, we took advantage of our unique *in vivo* model to examine

165 the impact of miransertib in the dynamic pathophysiology of PI3K-driven vascular malformations.

166 Previous preclinical studies of miransertib using tumor xenografts showed that the minimum dose

167 that has an impact on tumour volume is 75 mg/kg (Yu *et al*, 2017); thus, we first evaluated this

168 dose to assess miransertib for preventing the formation of *Pik3ca*-driven vascular malformations.

169 For this, we treated P1 EC-Pik3ca$^{WT/H1047R}$ mice with 4-OHT and we dosed these mice with either

170 75 mg/kg of miransertib or vehicle at P1 and P2, followed by the analysis of P6 retinas (Fig 4A).

171 Miransertib prevented the formation of vascular malformations, assessed by the vascular area

172 and total EC number (Fig 4B, D, E) by inhibiting *Pik3ca*^{H1047R}-driven EC hyperproliferation

173 assessed by EdU incorporation (Fig 4B, F). Also, treatment prevented the loss of NG2-positive

174 mural cell coverage (Fig EV4). By using pS6 immunostaining, we confirmed that miransertib

175 treatment inhibited PI3K signalling in the vasculature (Fig 4C, G). Of note, wild type control retinas

176 treated with miransertib showed a slight impact on vasculature density and EC proliferation (Fig

177 4B, D, F) further supporting a key role of AKT in angiogenesis and vascular homeostasis (Kerr *et*

178 *al*, 2016; Ackah *et al*, 2005; Chen *et al*, 2005).

179   Molecularly targeted treatment of vascular malformations might require long-term, even

180 chronic, therapeutic approaches in paediatric patients. This points to the importance of identifying

181 the minimal effective dose of any candidate treatment. Thus, we next asked whether reducing the

182 dose of miransertib would provide similar efficacy and reduce knock-on effects on normal

183 vasculature in our preclinical model. To test this, we reduced miransertib dose by half (35 mg/kg)

184 and evaluated its efficacy on preventing *Pik3ca*-driven vascular malformations (Fig 5A). We

185 observed that the therapeutic efficacy of AKT inhibition by miransertib was maintained at the lower

186 dose, with decreased EC proliferation leading to reduced number of total ECs and vascular

187 density in EC-*Pik3ca*^{H1047R} miransertib-treated retinas compared to vehicle-treated counterparts

188 (Fig 5B, D-F). Low dose of miransertib efficiently inactivated PI3K signalling as shown by reduced

189   pS6 levels (Fig 5C, G). Importantly, this minimum effective dose had no impact on non-mutant

190   vasculature (Fig 5B-G). Altogether, our data demonstrate that miransertib efficiently inhibits the

191   formation of PI3K-driven vascular malformations and that lower doses than reported for

192   oncological purposes of miransertib appear equally effective for preventive strategies.

193

194   ***Treatment with low dose of miransertib induces the regression of PI3K-driven vascular***

195   ***malformations***

196   Since vascular malformations are congenital diseases, therapeutic interventions should aim

197   for inducing the regression of mass lesions. In line with this, we assessed the therapeutic effect

198   of low dose miransertib on PI3K-driven vascular malformations. For this, we first induced the

199   formation of vascular malformations by treating EC-*Pik3ca*^WT/H1047R mice with 4-OHT at P1 and

200   then treat these mice with 35 mg/kg (low dose) of miransertib at P4 and P5 (Fig 6A). Of note, in

201   our *in vivo* preclinical model, vascular malformations are already present at P4 (Fig EV6), showing

202   all hallmarks of PI3K-driven vascular malformations: increased vascularity (Fig EV6B, F), number

203   of ECs (Fig EV6C, G), EC hyperproliferation (Fig EV6C, H), enhanced pS6 levels (Fig EV6D, I)

204   and impaired pericyte coverage (Fig EV6E, J). In contrast to vehicle-treated, miransertib

205   treatment of EC-*Pik3ca*^H1047R retinas effectively regressed vascular malformations, assessed by

206   the normalisation of the vascular density, EC numbers, and proliferation rate (Fig 6B, D-F).

207   Importantly, elevated PI3K signalling induced by *Pik3ca*^H1047R was eficiently blunted by miransertib

208   (Fig 6C, G). These data demonstrate that low dose miransertib is effective in inducing regression

209   of PI3K-driven vascular malformations; hence opening a very promising clinical strategy for these

210   diseases.

211

212   ***Miransertib inhibits PI3K/AKT signalling and reduces cell viability in patient-derived***

213   ***PIK3CA- and TEK-mutant endothelial cells***

214   Next, we assessed the therapeutic potential of miransertib in a preclinical human setting. For

215   this, we isolated and cultured ECs derived from human vascular malformations carrying mutations

216   in *PIK3CA* and *TEK/TIE2* (Appendix Table S1), spanning the genetic causes of more than 80%

217   of low-flow lesions in patients (Castillo *et al*, 2016a; Castel *et al*, 2016; Limaye *et al*, 2015; Limaye

218   *et al*, 2009). To isolate and culture these cells, fresh surgical resections of low-flow vascular

219   malformations were subjected to tissue digestion and EC positive selection (Fig 7A). Sanger

220   sequencing and droplet digital PCR revealed that causing mutations were present in the EC

221   culture, with variant allelic frequencies (VAFs) of around 50% in these cell cultures (Fig 7B;

222   Appendix Fig S1A,B). Characterization of these cells validated their specific EC properties –

223   cobblestone morphology and expression of the EC-specific markers VE-cadherin and ERG (Fig

224   7C; Appendix Fig S1C). Next, we analysed the impact of these mutations in PI3K signalling by

225   assessing AKT and S6 phosphorylation levels. Indeed, *PIK3CA*- and *TIE2*-mutant ECs exhibited

226   constitutive activation of the pathway compared with wild type HUVECs (Fig 7D). To evaluate the

227   therapeutic efficacy of miransertib in patient-derived *PIK3CA* and *TEK* mutant ECs, we first

228   assessed its impact on PI3K/AKT signalling. At very low doses, miransertib strongly inhibited AKT

229   signalling assessed by AKT and S6 phosphorylation levels that were reduced in a dose-

230   dependent manner. This effect was similar in both *PIK3CA* and *TEK* mutant ECs (Fig 7E, F). We

231   then studied the functional impact of miransertib-mediated AKT signalling inhibition by

232   determining the dose-response effect on cell viability in ECs with either *PIK3CA*- or *TEK*-mutant

233   genotype. Miransertib robustly decreased EC viability in both genotypes showing low IC_{50} with

234   overlaping (not significantly different) confident intervals (Fig 7G). These data show that

235   miransertib impacts the viability of patient-derived ECs at low concentrations and that it might

236   constitute a promising therapeutic strategy for both *PIK3CA* and *TEK*-mutant vascular

237   malformations.

Discussion

238

239   Activation of the PI3K/AKT signalling pathway by genetic mutations in the endothelium is the

240   primary etiological cause of most, if not all, low-flow vascular malformations (Castillo *et al*, 2016a;

241   Castel *et al*, 2016; Limaye *et al*, 2015; Boscolo *et al*, 2015; Luks *et al*, 2015). Despite of this, there

242   is no molecular targeted therapy approved for their clinical management today. Using the

243   postnatal mouse retina as a model of vascular malformations in combination with a tamoxifen-

244   induced strategy which allows to mosaically express the activating H1047R *Pik3ca* mutation at

245   different developmental times, we demostrate that active angiogenesis is required for *Pik3ca*

246   mutants to generate vascular malformations. Here we report on an optimised, robust, and efficient

247   preclinical system displaying traits constituting the main hallmarks of low-flow blood vascular

248   malformations' pathogenesis: overactivation of PI3K signalling, low-flow vascular compartment

249   specificity, loss of mural cell coverage, and EC hyperproliferation. With this model we show that

250   low dose miransertib effectively target these hallmarks preventing and inducing the regression of

251   already formed vascular malformations driven by *Pik3ca* overactivation.

252   Low-flow vascular malformations are congenital diseases therefore causative mutations occur

253   during embryonic development (Pang *et al*, 2020). However, the mechanisms of how mutations

254   result in a malformed vascular bed remained elusive. Our results demonstrate that activating

255   *Pik3ca* mutations in ECs are not sufficent for a malformed vascular lesion to appear and that a

256   burst of growth factor signals is essential to generate and expand them. Indeed, we demonstrate

257   that *Pik3ca*-related vascular malformations *in vivo* form via EC hyperproliferation during active

258   angiogenesis. In line with this, cultured *TEK* or *PIK3CA* mutant endothelial cells lead to

259   pathological proliferative response only upon stimulation of growth signals (Cai *et al*, 2019; Le

260   Cras *et al*, 2020). Also, *in vivo*, other types of PI3K-related vascular malformations such as

261   *Pik3ca*-driven lymphatic malformations or hereditary hemorrhagic telangiectasia-like

262   arteriovenous malformations rely on growth factor signals to be induced and expand (Mäkinen *et*

263   *al*, 2021; Martinez-Corral *et al*, 2020; Garrido-Martin *et al*, 2014). Another important observation

264   of our model is that *Pik3ca*-related blood vascular malformations only occur in veins and in the

265   capillary bed, excluding arteries which remain unaltered. This resembles the human spectrum of

266 vascular malformations where *PIK3CA* mutations have not been reported in arterial

267 malformations. Why arteries are unaffected by *Pik3ca* mutation remains unclear. This could be

268 related to the refractory behaviour that arterial cells exhibit upon reaching their definitive

269 maturation state (Orsenigo *et al*, 2020; Luo *et al*, 2021) and the cell cycle arrested state which

270 fluid shear stress imposes on arterial ECs (Fang *et al*, 2017).

271 The growth-push concept fits with clinical observations where low-flow vascular malformations

272 appear during embryonic development, expand proportionally with the physiological growth of the

273 patient and are largely quiescent during adulthood, when the production of growth factors is

274 residual (Pang *et al*, 2020). This also explains why low-flow vascular malformations are

275 histopathologically characterized by a low rate of EC proliferation (Castillo *et al*, 2016b). However,

276 despite of being considered as non-proliferative lesions at the time of diagnosis, acute production

277 of extrinsic inputs such as hormonal changes, injury, or wound healing, reactivate malformed

278 vasculature (Pang *et al*, 2020); thereby being a key aspect to mind for preventive approaches. In

279 fact, this may explain why lesions recur upon incomplete surgical removal when wound healing

280 signals are acutely produced. Collectively, our data suggest that blocking EC growth should be

281 considered during potential reactivation scenarios. Furthermore, our study calls for revisiting

282 current classification of low-flow vascular malformation which should be considered proliferative

283 vascular disorders.

284 Inhibition of the PI3K/AKT signalling pathway has been prioritised in targeted therapy

285 strategies in medical oncology (Vanhaesebroeck *et al*, 2021; Castel *et al*, 2021). However, for

286 vascular malformations there is no molecular therapy approved in the clinic today. This is

287 surprising given that *PIK3CA* oncogenic mutations causing vascular malformations are also

288 present in epithelial cancer (Samuels *et al*, 2004). At least in part, the lack of robust and rapid

289 preclinical models for drug evaluation has hampered the field. In this study, we provide evidence

290 that the mouse retina model offers an opportunity for preclinical drug testing of blood vascular

291 disorders. The key aspects of this model are: (i) it develops in a short time frame (one week); (ii)

292 it allows for a dynamic preclinical testing which covers prevention and curative strategies; (iii) it

293 grants the quantification of disease hallmarks including vascularity, EC proliferation and PI3K

294   signalling, thus providing a robust and non-biased setting to evaluate treatment efficacy; (iv) it

295   recapitulates relevant features of vascular malformations microenvironment including the impact

296   of blood flow, extracellular matrix, surrounding pericytes, and smooth muscle cells, which may

297   influence drug response. Of relevance, this experimental system has been previously used for

298   targeted therapy validation in other vascular disorders (Ola *et al*, 2018, 2016; Alsina-Sanchis *et*

299   *al*, 2018). Importantly, our model takes into account the mosaic and focal nature of the disease,

300   in which vascular malformations arise in an otherwise normal vasculature network. Thus,

301   preclinical analysis in isolated and focal vascular malformations embedded in a normal vascular

302   plexus allows the study of the impact of drugs in both the lesion and the normal vasculature. This

303   permits the identification of potential knock-on effects of compounds in the systemic vasculature.

304   All in all, we propose mouse retinas as the standard pre-clinical model for low-flow blood vascular

305   malformations.

306   Blocking AKT signalling has been a promising therapy for cancer; however, rewiring PI3K

307   signalling due to the complex genetic landscape and instability of malignant cells have dampened

308   these expectations (Jansen *et al*, 2016). In contrast, vascular malformations are considered

309   monogenic diseases caused by activating point mutations in an otherwise stable genetic context

310   (Castel *et al*, 2020). These mutations cause an overactivation of the PI3K pathway by constitutive

311   phosphorylation of wild type AKT. Miransertib is a pan-AKT allosteric inibitor and has been shown

312   as a promising AKT inhibitor in preclinical and clinical studies (Lazaro *et al*, 2020) by inhibiting

313   overactive wild-type AKT (Kostaras *et al*, 2020). This therapeutic approach has proven to be

314   efficent in preclinical models of cancer (Yu *et al*, 2017) and in Proteus syndrome, caused by the

315   mosaic expression of an activating *AKT1* mutation (Biesecker *et al*, 2020; Lindhurst *et al*, 2015).

316   Of relevance, miransertib has shown clinical benefit in two children with PROS (Forde *et al*, 2021).

317   Altogether, it has led to the current phase 1/2 clinical trial (NCT03094832) for the assessment of

318   miransertib in Proteus and PROS patients. Based on this, we aimed at assessing the impact of

319   miransentib as a novel treatment for isolated low-flow blood vascular malformations. This seems

320   particulary relevant for those patients in which PI3K inhibitors cause severe side effects due to

321   the pleiotropic functions of PI3K. Here, we provide the first *in vivo* demonstration of miransertib

322   efficacy in PI3K-driven vascular malformations. Our data indicate that, similar to alpelisib, a

323   selective p110α inhibitor, low dose miransertib is sufficent to prevent and induce complete

324   regression of these diseases (Venot *et al*, 2018). We anticipate that these results will have a direct

325   impact on future clinical strategies. Indeed, these patients may need long-term or even chronic

326   treatment; thus an effective low dose may turn specially relevant to avoid undesirable side effects

327   for paediatric age patients.

328   To complement our *in vivo* preclinical approach, we have set up the isolation and culture of

329   human primary ECs from low-flow vascular lesions. On average, these cultures showed a 50%

330   allelic frequency of *PIK3CA*- or *TEK*-mutant allelels which is suggestive of clonal culture and

331   expansion. Of note, all human cells exhibited overactivation of AKT compared to non-mutant cells,

332   although with allele differences. This unique material turns really valuable to test the impact of

333   targeted therapies. In this regard, we demonstrate that miransertib similarly impairs cell viability

334   of *PIK3CA*- and *TEK*-mutant ECs derived from patients. This is in line with previous studies

335   reporting the effect of miransertib in *PIK3CA*-mutant endothelial cells (Boscolo *et al*, 2019). Our

336   results might indicate that this therapy is also effective for *TEK*-mutant vascular malformations;

337   however, the lack of *TEK*-mutant mouse lines precludes the assessement *in vivo*.

338   The discovery that most low-flow lesions are caused by the overactivation of PI3K signalling

339   has catalysed the repurpose of PI3K pathway inhibitors for these diseases. In order to promote

340   their direct clinical application, the field urgently needs reliable preclinical models before and while

341   clinical trials are running in humans. By using mouse retinas, we solve this limitation while

342   providing formal proof that low dose miransertib is sufficent to prevent and treat *Pik3ca*-related

343   vascular malformmations. Complementing these data with primary human ECs offers a unique

344   opportunity for personalized medicine.

345 **Materials and Methods**

346 *Reagents*

347 All chemical reagents were purchased from Sigma-Aldrich, unless stated otherwise. Cell culture

348 media and buffers were purchased from Lonza and Gibco. Primers were obtained from Invitrogen.

349 *Mice*

350 The *in vivo* experiments were performed in agreement with the guidelines and legislations of the

351 Catalan Ministry of Agriculture, Livestock, Fisheries and Food (Catalonia, Spain), following

352 protocols approved by the local Ethics Committees of IDIBELL-CEEA. Mice were kept in

353 individually ventilated cages under specific pathogen-free conditions. All mice were crossed onto

354 the C57BL/6J genetic background. *Pik3ca*$^{WT/H1047R}$ mice carry a single, germline Cre-inducible

355 point mutation in *Pik3ca* allele (H1047R) (Kinross *et al*, 2012). This mice are crossed onto *Pdgfb*-

356 iCreER mice (Claxton *et al*, 2008) that express an inducible iCreER recombinase from the

357 endogenous *Pdgfb* locus (EC specific). Control mice were CreiER-negative littermates injected

358 with 4-hydroxytamoxifen. iCreER-mediated recombination in *Pik3ca*$^{WT/H1047R}$ mice was induced by

359 intraperitoneal injection of 4-hydroxytamoxifen (doses indicated in the figure legends). ROSA-

360 mTmG double fluorescent reporter mouse (Muzumdar *et al*, 2007) was crossed to *Pdgfb*-iCreER

361 mice. The ROSA-mTmG allele was kept heterozygous. 4-Hydroxytamoxifen was injected

362 intraperitoneally in indicated doses (see the figure legends) and mouse retinas isolated at

363 indicated time points. Cre-mediated recombination was assessed by the expression of

364 membrane-bound GFP.

365 *Pharmacological in vivo treatment*

366 Miransertib (ARQ 092·2MSA salt) (ArQule, Inc., a wholly-owned subsidiary of Merck & Co., Inc.,

367 Kenilworth, NJ, USA) was prepared at a stock concentration of 10 mgA/ml in 20% Captisol (m/v)

368 in 0.02 M citrate/saline buffer. 20% Captisol (m/v) in 0.02 M citrate/saline buffer was used as a

369 vehicle. Mice were injected intraperitoneally with either 75 mg/kg or 35 mg/kg dose of miransertib.

370 *Mouse retina isolation and immunostaining*

371 Mice were sacrificed by decapitation and eyes were isolated, followed by an hour incubation on

372 ice in 4% PFA in PBS. Isolated retinas were fixed for additional hour, permeabilised overnight at

373   4°C in permabilisation/blocking buffer (1% BSA, 0.3% Triton X-100 in PBS). Afterwards, the

374   retinas were incubated overnight at 4°C with specific primary antibodies, diluted in

375   permabilisation/blocking buffer (ERG (Abcam, AB92513, diluted 1:400), NG2 (Milipore, AB5320,

376   diluted 1:200), p-S6 235/236 (Cell Signalling Technology, 4857, diluted 1:100). Samples were

377   washed three times in PBS contraining 1% Tween-20 (PBST), following incubation with PBlec

378   buffer (1% Triton X- 100, 1 mM $CaCl_2$, 1 mM $MgCl_2$ and 1 mM $MnCl_2$ in PBS, pH 6.8) for 30

379   minutes at RT. Secondary AlexaFluor-conjugated antibodies, diluted in PBlec, were added to the

380   retinas and incubated for another 2 hours (Invitrogen, A11001, A11011, A11008, A31573). Blood

381   vessels were visualised with AlexaFluor-conjugated Isolectin GS-B4 (Molecular Probes, I21411,

382   I21412). Following three washes with PBST, the tissues were flat-mounted on a microscope slide.

383   ***In vivo proliferation assay***

384   5-ethynyl-2'-deoxyuridine (EdU)-incorporation assay has been performed using a commercially

385   available kit (Invitrogen, C10340). Animals were injected intraperitoneally with 60 μl of EdU (0.5

386   mg/ml in 50% DMSO and 50% PBS solution) and after 2 hours the animals were sacrificed and

387   retinas isolated. EdU-incorporation was detected with Click-iT EdU Alexa Fluor-647 Imaging Kit,

388   following manufactures instructions. Afterwards, standard protocol for retina immunostaining was

389   applied.

390   ***Confocal imaging and image quantification***

391   Microscopy imaging was done with Leica TCS SP5 confocal microscope. Volocity, Adobe

392   Photoshop 2021 and ImageJ softwares were used for image editing and quantification,

393   respectively. Images were taken from at least 4 retina areas in each genotype. At least three

394   biological replicates per genotype were performed. To quantify the vascular lesion area, an IB4-

395   positive area was manually selected and the percentage of IB4 area per retina area was

396   quantifed. To determine the recombination efficiency of mTmG allele in ECs, the ratio of GFP-

397   positive area to IB4-positive area was calculated and presented as percentage. Retina vascularity

398   was measured using IB4 channel by adjusting the threshold to select the IB4-positive area,

399   followed by quantification of the percentage of IB4-positive area in the total image area (10^4 μm^2).

400   EC number was determined manually based on EC-specific nuclei staining (Erg) in 10^4 μm^2 image

401 area. Quantification of EC proliferation was done using EdU and Erg co-immunostaining – both

402 EdU- and Erg-positive ECs were quantified in the 10^4 μm^2 image area. The coverage of vessels

403 by NG2-positive pericytes was quantified from both NG2 and IB4 channels by adjusting the

404 threshold and selecting the positive NG2 and IB4 areas, respectively. Then the percentage of

405 NG2 to IB4 ratio was calculated. The vascular-specific p-S6 intensity was measured using both

406 p-S6 and IB4 channels. First, a manual threshold was set to obtain the IB4-positive area and

407 define the region of interest (ROI). Then, the integrated density of p-S6 was measured in IB4-

408 positive areas. The background measurements (mean gray values) were taken from areas in

409 close proximity to the vasculature, but negative for IB4. The corrected total fluorescence (CTF)

410 was calculated based on the following equation: CTF = integrated density – (vascular area ×

411 mean gray background value).

412 ***Isolation, culture and sequencing of endothelial cells from patient-derived vascular***

413 ***malformations***

414 Patient tissue samples were obtained under therapeutic surgical resection from participants after

415 informed consent with approval of the Committees on Biomedical Investigation at Hospital Sant

416 Joan de Deu and Hospital Santa Creu i Sant Pau (Barcelona, Spain). Collected data were stored

417 in a secure database maintained by Hospital Sant Joan de Deu. Human ECs were isolated from

418 patient-derived biopsies of vascular malformations. Briefly, the biopsy was homogenized with a

419 scalpel blade and digested in dispase II (4 U/ml) and collagenase A (0.9 mg/ml) in Hank's

420 Balanced Salt Solution for maximum 1.5 hour at 37°C, vortexing the sample every 30 minutes.

421 The digested tissue was disintegrated by pipetting into a single-cell solution, following enzyme

422 inactivation with DMEM supplemented with 10% FBS and 1% penicillin/streptomycin. Cells were

423 resuspended in 100 μl of 0.5% BSA in PBS and incubated with mouse anti-human CD31 (Agilent

424 Dako, M0823, clone JC70A) antibody-coated magnetic beads (ThermoFisher Scientific, 11041)

425 for 1 hour at room temperature. CD31-positive fraction was washed with 0.5% BSA in PBS and

426 sorted with a magnet. Cells were resuspended and cultured in 0.5% gelatin-coated culture well

427 (12-well format) in EGM2 medium (PromoCell, C30140) supplemented with 10% FBS, 1%

428 penicillin/streptomycin (later referred to as EGM2 complete) at 37°C and 5% CO_2 until they reach

429   confluency. Cells were subjected for a second selection. Genomic DNA was isolated according

430   to the manufacturer´s protocol (Thermo Fisher Scientific, K182001). The regions of interest in the

431   genomic DNA were amplified by PCR using Platinum™ Taq DNA Polymerase High Fidelity

432   (Thermo Fisher Scientific, 11304011). Exons 10 and 21 of *PIK3CA*, and exon 17 of *TEK* were

433   amplified. PCR products were purified according to the manufacture´s protocol (GE Healthcare,

434   28-9034-70) followed by Sanger sequencing. Sequences of the primers used: *PIK3CA* exon 10:

435   (forward)   5´-TGGTTCTTTCCTGTCTCTGAAAA-3´   and   (reverse)   5´-

436   CCATTTTAGCACTTACCTGTGAC-3´.   *PIK3CA*   exon   21:   (forward)   5´-

437   CATTTGCTCCAAACTGACCA-3´ and (reverse) 5´-TGTGTGGAAGATCCAATCCA-3´. *TEK* exon

438   17:   (forward)   5´-TAGGCAATTTCCACAGCACA-3´   and   (reverse)   5´-

439   GGCAAACCAGGCTAAGAGAG-3´. Droplet digital PCR was done on genomic DNA extracted

440   from cell cultures. *PIK3CA* genotyping assays from Bio-Rad were used to specifically detect the

441   *PIK3CA^E542K^* mutation on DNA samples. The Bio-Rad QX200 ddPCR system was used and allelic

442   frequencies were calculated using Quantasoft Analysis Pro (BioRad) software.

Cell immunofluorescence

444   Human VM-derived ECs were seeded on gelatin-coated coverslips in a way to reach confluency

445   the next day and incubated overnight at 37°C in 5% CO_2. Then, cells were washed with warm

446   PBS with Mg^{2+} and Ca^{2+} then fixed with 4% PFA for 15 minutes at room temperature, followed by

447   triple wash with PBS with Mg^{2+} and Ca^{2+}. Cells were permeabilised with PBS containing 0.4%

448   Triton X-100 for 5 minutes and blocked with 2% BSA in PBS for 1 hour at RT. The following

449   primary antibodies were used for 1h at RT: VE-cadherin F8 (Santa Cruz, SC-9989, 1:100), ERG

450   (Abcam, ab92513, 1:400). Then, coverslips were washed three times with PBS for 5 minutes,

451   followed by 45 min incubation at RT with appropriate secondary antibody in PBS: goat anti-mouse

452   Alexa Fluor-488 (Invitrogen A11001, diluted 1:300) and goat anti-rabbit Alexa Fluor-568

453   (Invitrogen A11011, diluted 1:300). Then, coverslips were washed with PBS three times for 5 min,

454   and in the last wash DAPI (Invitrogen, D1306, diluted 1:10 000) was added to visualize cell nuclei.

455   Coverslips were mounted on a microscope slide in a mounting medium (ThermoFisher Scientific,

456   9990402).

457   ***MTS viability assay and calculation of IC50***

458   MTS assay was used in order to determine cell viability. Briefly, $2 \cdot 10^3$ cells were seeded on

459   gelatin-coated 96-well plates (5 technical replicates per condition) and incubated overnight at

460   37°C in 5% CO_2 atmosphere. The next day, cells were treated for 3 days with miransertib. MTS

461   assay (Abcam, ab197010) was performed for 2.5 hours and the absorbance was measured at

462   490 nm. Data (the percentage of a vehicle) were plotted against the logarithm of inhibitor

463   concentration. IC50 and 95% CI values were calculated by non-linear regression (variable slope)

464   using GraphPad Prism software.

465   ***Protein extraction and immunoblotting***

466   Cells were lysed in ice cold lysis buffer (50 mM Tris-HCl pH 7.4, 5 mM EDTA, 150 mM NaCl and

467   1% Triton X-100) containing protease (Roche, 11836153001) and phosphatase inhibitors (Sigma-

468   Aldrich, 4906837001). Total cell lysates were resolved on 10% polyacrylamide gels, transferred

469   onto nitrocellulose membranes and incubated with appropriate primary and secondary antibodies.

470   The following primary antibodies were used: p-AKT S473 (CST, 4060, diluted 1:1000), p-AKT

471   T308 (CST, 4056S, diluted 1:500), AKT (CST, 9272, diluted 1:2000), p-S6 S235/236 (CST, 4857,

472   diluted 1:1000), p-S6 S240/244 (CST, 2215S, diluted 1:1000), S6 (CST, 2212, diluted 1:1000),

473   VE-cadherin (Santa Cruz Biotechnology, sc-6458, diluted 1:500), vinculin (Abcam, ab49900,

474   diluted 1:10000). The following secondary antibodies from DAKO were used (all diluted 1:5000):

475   swine anti-rabbit (P0399), rabbit anti-goat (P0449), rabbit anti-mouse (P0260), and rabbit anti-

476   sheep (P0163).

477   ***Statistics***

478   Statistical analysis was performed by a nonparametric Mann Whitney's test using Prism 8

479   (GraphPad Software Inc.) unless indicated otherwise. All figures are displayed with individual data

480   points that indicate biological replicates and with the standard error of the mean (s.e.m.) as errors

481   bars. At least 3 biological replicates were used. P values considered as statistically significant

482   were as follows: *$p < 0.05$; **$p < 0.01$ and ***$p < 0.0001$.

Acknowledgements

502

Author contribution

503

504   M.G., S.D.C., P.K and H.S. were the main contributors in the conception, design, acquisition, and

505   interpretation of the data and in writing the article. P.K. H.S, O.V., A.A-U., L.M., J.Z., N.G. O., C.L.

506   and S.D.C. performed experiments and data analysis with input from S.D.C. and M.G.. C.R. and

507   O.M-A. interpreted histopathology. V.C., S.L., E.B and J.M. liaised with human subjects and

508   provided access to human tissue samples and clinical input in the study.

509   **Conflict of interest**

510   M.G. has a research agreement with ArQule, Inc., a wholly-owned subsidary of Merck & Co.,

511   Inc., Kenilworth, NJ, USA, and Venthera. E.B. is founder and CAB of Venthera; PI and Advisor

512   for Pierre Fabre; PI of the clinical trial NCT04589650 (Novartis).

513

514   **The Paper Explained**

515   PROBLEM: Low-flow vascular malformations are congenital diseases caused by a focal

516   overgrowth of vessels. They may cause pain, bleeding, infections, and obstruction of organs.

517   Despite that their genetic causes are known for some years, which lead to the hyperactivation of

518   PI3K signalling, at present there is no molecular targeted therapy approved for these diseases.

519   RESULTS: We have generated a robust and fast preclinical *in vivo* model that allows for testing

520   of targeted drugs. With this model we have demonstrated that PI3K-driven vascular

521   malformations rely on active angiogenesis to occur. Our preclinical studies show that AKT

522   inhibition using low dose miransertib prevents the disease and fully regresses established

523   vascular malformations.

524   IMPACT: Our new *in vivo* model of PI3K-driven vascular malformations is a reliable and fast

525   preclinical setting to test new or repurposed targeted drugs. Our studies support that *Pik3ca*-

526   mutant endothelial cells cause vascular malformations upon growth stimuli highlighting the

527   importance of preventive therapeutic approaches after invasive treatments. We provide proof of

528   concept for the use of the AKT inhibitor miransertib in PI3K-driven vascular malformations which

529   opens a new window for targeted therapeutic intervention for these diseases. Also, we

530   demonstrate *in vitro* that this targeted therapy is similarly effective in both *PIK3CA* and *TEK*-

531   mutant vascular malformations.

References

Ackah E, Yu J, Zoellner S, Iwakiri Y, Skurk C, Shibata R, Ouchi N, Easton RM, Galasso G, Birnbaum MJ, et al (2005) Akt1/protein kinase Bα is critical for ischemic and VEGF-mediated angiogenesis. *J Clin Invest* 115: 2119–2127

Alsina-Sanchis E, Garcia-Ibanez Y, Figueiredo AM, Riera-Domingo C, Figueras A, Matias-Guiu X, Casanovas O, Botella LM, Pujana MA, Riera-Mestre A, et al (2018) ALK1 loss results in vascular hyperplasia in mice and humans through PI3K activation. *Arterioscler Thromb Vasc Biol* 38: 1216–1229

Biesecker LG, Edwards M, O'Donnell S, Doherty P, MacDougall T, Tith K, Kazakin J & Schwartz B (2020) Clinical report: One year of treatment of Proteus syndrome with miransertib (ARQ 092). *Cold Spring Harb Mol Case Stud* 6: a004549

Bilanges B, Posor Y & Vanhaesebroeck B (2019) PI3K isoforms in cell signalling and vesicle trafficking. *Nat Rev Mol Cell Biol* 20: 515–534

Boscolo E, Coma S, Luks VL, Greene AK, Klagsbrun M, Warman ML & Bischoff J (2015) AKT hyper-phosphorylation associated with PI3K mutations in lymphatic endothelial cells from a patient with lymphatic malformation. *Angiogenesis* 18: 151–162

Boscolo E, Pastura P, Glaser K, Goines J, Hammill AM, Adams DM, Dickie P, Hsi Dickie B & Le Cras TD (2019) Signaling pathways and inhibitors of cells from patients with kaposiform lymphangiomatosis. *Pediatr Blood Cancer* 66: e27790

Cai Y, Schrenk S, Goines J, Davis GE & Boscolo E (2019) Constitutive Active Mutant TIE2 Induces Enlarged Vascular Lumen Formation with Loss of Apico-basal Polarity and Pericyte Recruitment. *Sci Rep* 9:12352

Canaud G, Hammill AM, Adams D, Vikkula M & Keppler-Noreuil KM (2021) A review of mechanisms of disease across PIK3CA-related disorders with vascular manifestations. *Orphanet J Rare Dis* 16: 306

Castel P, Carmona FJ, Grego-Bessa J, Berger MF, Viale A, Anderson K V., Bague S, Scaltriti M, Antonescu CR, Baselga E, et al (2016) Somatic PIK3CA mutations as a driver of sporadic venous malformations. *Sci Transl Med* 8: 332ra42

560   Castel P, Rauen KA & McCormick F (2020) The duality of human oncoproteins: drivers of cancer

561   and congenital disorders. *Nat Rev Cancer* 20: 383–397

562   Castel P, Toska E, Engelman JA & Scaltriti M (2021) The present and future of PI3K inhibitors for

563   cancer therapy. *Nat Cancer* 2: 587–597

564   Castillo SD, Baselga E & Graupera M (2019) PIK3CA mutations in vascular malformations. *Curr*

565   *Opin Hematol* 26: 170–178

566   Castillo SD, Tzouanacou E, Zaw-Thin M, Berenjeno IM, Parker VER, Chivite I, Milà-Guasch M,

567   Pearce W, Solomon I, Angulo-Urarte A, et al (2016a) Somatic activating mutations in Pik3ca

568   cause sporadic venous malformations in mice and humans. Sci Transl Med 8: 332ra43

569   Castillo SD, Vanhaesebroeck B & Sebire NJ (2016b) Phosphoinositide 3-kinase: a new kid on the

570   block in vascular anomalies. *J Pathol* 240: 387–396

571   Chen J, Somanath PR, Razorenova O, Chen WS, Hay N, Bornstein P & Byzova T V. (2005) Akt1

572   regulates pathological angiogenesis, vascular maturation and permeability in vivo. *Nat Med*

573   11: 1188–1196

574   Claxton S, Kostourou V, Jadeja S, Chambon P, Hodivala-Dilke K & Fruttiger M (2008) Efficient,

575   inducible cre-recombinase activation in vascular endothelium. *Genesis* 46: 74–80

576   Le Cras TD, Goines J, Lakes N, Pastura P, Hammill AM, Adams DM & Boscolo E (2020)

577   Constitutively active PIK3CA mutations are expressed by lymphatic and vascular endothelial

578   cells in capillary lymphatic venous malformation. *Angiogenesis* 23: 425–442

579   Van Damme A, Seront E, Dekeuleneer V, Boon LM & Vikkula M (2020) New and Emerging

580   Targeted Therapies for Vascular Malformations. *Am J Clin Dermatol* 21: 657–668

581   Ehling M, Adams S, Benedito R & Adams RH (2013) Notch controls retinal blood vessel

582   maturation and quiescence. *Dev* 140: 3051–3061

583   Fang JS, Coon BG, Gillis N, Chen Z, Qiu J, Chittenden TW, Burt JM, Schwartz MA & Hirschi KK

584   (2017) Shear-induced Notch-Cx37-p27 axis arrests endothelial cell cycle to enable arterial

585   specification. *Nat Commun* 8: 2149

586   Forde K, Resta N, Ranieri C, Rea D, Kubassova O, Hinton M, Andrews KA, Semple R, Irvine AD

587   & Dvorakova V (2021) Clinical experience with the AKT1 inhibitor miransertib in two children

588   with PIK3CA-related overgrowth syndrome. *Orphanet J Rare Dis* 16: 109

589   Garrido-Martin EM, Nguyen HL, Cunningham TA, Choe SW, Jiang Z, Arthur HM, Lee YJ & Oh

590   SP (2014) Common and distinctive pathogenetic features of arteriovenous malformations in

591   hereditary hemorrhagic telangiectasia 1 and hereditary hemorrhagic telangiectasia 2 animal

592   models - Brief report. Arterioscler Thromb Vasc Biol 34: 2232–2236

593   Graupera M, Guillermet-Guibert J, Foukas LC, Phng LK, Cain RJ, Salpekar A, Pearce W, Meek

594   S, Millan J, Cutillas PR, et al (2008) Angiogenesis selectively requires the p110α isoform of

595   PI3K to control endothelial cell migration. *Nature* 453: 662–666

596   Graupera M & Potente M (2013) Regulation of angiogenesis by PI3K signaling networks. *Exp Cell*

597   *Res* 319: 1348–1355

598   Jansen VM, Mayer IA & Arteaga CL (2016) Is there a future for AKT inhibitors in the treatment of

599   cancer? *Clin Cancer Res* 22: 2599–2601

600   Keppler-Noreuil KM, Rios JJ, Parker VER, Semple RK, Lindhurst MJ, Sapp JC, Alomari A, Ezaki

601   M, Dobyns W & Biesecker LG (2015) PIK3CA-related overgrowth spectrum (PROS):

602   Diagnostic and testing eligibility criteria, differential diagnosis, and evaluation. *Am J Med Genet*

603   *Part A* 167: 287–295

604   Kerr BA, West XZ, Kim YW, Zhao Y, Tischenko M, Cull RM, Phares TW, Peng XD, Bernier-

605   Latmani J, Petrova T V., et al (2016) Stability and function of adult vasculature is sustained by

606   Akt/Jagged1 signalling axis in endothelium. *Nat Commun* 7: 10960

607   Kinross KM, Montgomery KG, Kleinschmidt M, Waring P, Ivetac I, Tikoo A, Saad M, Hare L, Roh

608   V, Mantamadiotis T, et al (2012) An activating Pik3ca mutation coupled with Pten loss is

609   sufficient to initiate ovarian tumorigenesis in mice. *J Clin Invest* 122: 553–557

610   Kobialka P & Graupera M (2019) Revisiting PI3-kinase signalling in angiogenesis. *Vasc Biol*

611   *(Bristol, England)* 1: H125–H134

612 Kostaras E, Kaserer T, Lazaro G, Heuss SF, Hussain A, Casado P, Hayes A, Yandim C, Palaskas

613   N, Yu Y, et al (2020) A systematic molecular and pharmacologic evaluation of AKT inhibitors

614   reveals new insight into their biological activity. *Br J Cancer* 123: 542–555

615 Lazaro G, Kostaras E & Vivanco I (2020) Inhibitors in AKTion: ATP-competitive vs allosteric.

616   *Biochem Soc Trans* 48: 933–943

617 Leoni C, Gullo G, Resta N, Fagotti A, Onesimo R, Schwartz B, Kazakin J, Abbadessa G, Crown

618   J, Collins CD, et al (2019) First evidence of a therapeutic effect of miransertib in a teenager

619   with Proteus syndrome and ovarian carcinoma. *Am J Med Genet Part A* 179: 1319–1324

620 Limaye N, Kangas J, Mendola A, Godfraind C, Schlögel MJ, Helaers R, Eklund L, Boon LM &

621   Vikkula M (2015) Somatic Activating PIK3CA Mutations Cause Venous Malformation. *Am J*

622   *Hum Genet* 97: 914–921

623 Limaye N, Wouters V, Uebelhoer M, Tuominen M, Wirkkala R, Mulliken JB, Eklund L, Boon LM

624   & Vikkula M (2009) Somatic mutations in angiopoietin receptor gene TEK cause solitary and

625   multiple sporadic venous malformations. *Nat Genet* 41: 118–124

626 Lindhurst MJ, Yourick MR, Yu Y, Savage RE, Ferrari D & Biesecker LG (2015) Repression of

627   AKT signaling by ARQ 092 in cells and tissues from patients with Proteus syndrome. *Sci Rep*

628   5: 17162

629 Luks VL, Kamitaki N, Vivero MP, Uller W, Rab R, Bovee JVMG, Rialon KL, Guevara CJ, Alomari

630   AI, Greene AK, et al (2015) Lymphatic and other vascular malformative/overgrowth disorders

631   are caused by somatic mutations in PIK3CA. *J Pediatr* 166: 1048-1054.e5

632 Luo W, Garcia-Gonzalez I, Fernández-Chacón M, Casquero-Garcia V, Sanchez-Muñoz MS,

633   Mühleder S, Garcia-Ortega L, Andrade J, Potente M & Benedito R (2021) Arterialization

634   requires the timely suppression of cell growth. *Nature* 589: 437–441

635 Mäkinen T, Boon LM, Vikkula M & Alitalo K (2021) Lymphatic Malformations: Genetics,

636   Mechanisms and Therapeutic Strategies. *Circ Res* 129: 136–154

637 Manning BD & Toker A (2017) AKT/PKB Signaling: Navigating the Network. *Cell* 169: 381–405

638   Martinez-Corral I, Zhang Y, Petkova M, Ortsäter H, Sjöberg S, Castillo SD, Brouillard P, Libbrecht

639   L, Saur D, Graupera M, et al (2020) Blockade of VEGF-C signaling inhibits lymphatic

640   malformations driven by oncogenic PIK3CA mutation. *Nat Commun* 11: 2869

641   Muzumdar MD, Tasic B, Miyamichi K, Li N & Luo L (2007) A global double-fluorescent cre reporter

642   mouse. *Genesis* 45: 593–605

643   Ola R, Dubrac A, Han J, Zhang F, Fang JS, Larrivée B, Lee M, Urarte AA, Kraehling JR, Genet

644   G, et al (2016) PI3 kinase inhibition improves vascular malformations in mouse models of

645   hereditary haemorrhagic telangiectasia. *Nat Commun* 7: 13650

646   Ola R, Künzel SH, Zhang F, Genet G, Chakraborty R, Pibouin-Fragner L, Martin K, Sessa W,

647   Dubrac A & Eichmann A (2018) SMAD4 Prevents Flow Induced Arteriovenous Malformations

648   by Inhibiting Casein Kinase 2. *Circulation* 138: 2379–2394

649   Orsenigo F, Conze LL, Jauhiainen S, Corada M, Lazzaroni F, Malinverno M, Sundell V, Cunha

650   SI, Brännström J, Globisch MA, et al (2020) Mapping endothelial-cell diversity in cerebral

651   cavernous malformations at single-cell resolution. *Elife* 9: e61413

652   Pang C, Lim CS, Brookes J, Tsui J & Hamilton G (2020) Emerging importance of molecular

653   pathogenesis of vascular malformations in clinical practice and classifications. *Vasc Med*

654   *(United Kingdom)* 25: 364–377

655   Samuels Y, Wang Z, Bardelli A, Silliman N, Ptak J, Szabo S, Yan H, Gazdar A, Powell SM, Riggins

656   GJ, et al (2004) High Frequency of Mutations of the PIK3CA Gene in Human Cancers. *Science*

657   304: 554

658   Stanczuk L, Martinez-Corral I, Ulvmar MH, Zhang Y, Laviña B, Fruttiger M, Adams RH, Saur D,

659   Betsholtz C, Ortega S, et al (2015) CKit lineage hemogenic endothelium-derived cells

660   contribute to mesenteric lymphatic vessels. *Cell Rep* 10: 1708–1721

661   Vanhaesebroeck B, Perry MWD, Brown JR, André F & Okkenhaug K (2021) PI3K inhibitors are

662   finally coming of age. *Nat Rev Drug Discov* Jun 14

663   Venot Q, Blanc T, Rabia SH, Berteloot L, Ladraa S, Duong JP, Blanc E, Johnson SC, Hoguin C,

664   Boccara O, et al (2018) Targeted therapy in patients with PIK3CA-related overgrowth

665   syndrome. *Nature* 558: 540–546

666   Yu Y, Hall T, Eathiraj S, Wick MJ, Schwartz B & Abbadessa G (2017) In-vitro and in-vivo combined

667   effect of ARQ 092, an AKT inhibitor, with ARQ 087, a FGFR inhibitor. *Anticancer Drugs* 28:

668   503–513

669   Yu Y, Savage RE, Eathiraj S, Meade J, Wick MJ, Hall T, Abbadessa G & Schwartz B (2015)

670   Targeting AKT1-E17K and the PI3K/AKT pathway with an allosteric AKT inhibitor, ARQ 092.

671   *PLoS One* 10: e0140479

Kobialka, Sabata et al.

672 **FIGURE LEGENDS**

673 **Figure 1. Pathogenesis of *Pik3ca*-driven vascular malformations depends on active**

674 **angiogenesis. (A)** Experimental setup scheme showing analysed angiogenic stages in the retina

675 models. (**B**) Representative images of control and EC-*Pik3ca*[H1047R/WT] mouse retinas isolated at

676 indicated time points stained with IB4 for blood vessels. Scale bars: 150 μm. (**C**) Pie charts

677 showing the incidence of vascular lesions at different angiogenic stages. Lesions were

678 categorised according to their expanse (generalised or focal). Quantification was performed per

679 retina petal. Numbers below show the presence of any type of lesions per retina petal. (**D**)

680 Quantification of IB4-positive areas per retina. Error bars are s.e.m. n ≥ 3 retinas per genotype.

681 (**E**) Representative images of EC-mTmG mouse retinas isolated at indicated time points stained

682 with IB4 and GFP. Scale bars: 150 μm. (**F**) Quantification of GFP/IB4 ratio per retina. Error bars

683 are s.e.m. n ≥ 3 retinas per genotype. Statistical analysis was performed by nonparametric Mann–

684 Whitney test. *p < 0.05 was considered statistically significant.

685 **Figure 2. Modelling PI3K-vascular malformations in murine retinas by mosaic expression**

686 **of Pik3ca[H1047R] in ECs. (A, B)** Representative images of EC-*Pik3ca*[H1047R/WT] (**A**) and EC-mTmG

687 (**B**) P6 retinas from mice treated with decreasing doses of 4-OHT on P1. Retinas were stained for

688 blood vessels (IB4) and GFP as indicated. Scale bars: 150 μm. (**C**) Quantification of GFP/IB4

689 ratio of EC-mTmG retinas. Error bars are s.e.m. n ≥ 3 retinas per genotype. (**D**) Quantification of

690 IB4-positive area per retina in *Pik3ca*[H1047R/WT] retinas. Data presented as a percentage of the

691 control for each 4-OHT dose. Error bars are s.e.m. n = 4 retinas per genotype. Statistical analysis

692 was performed by nonparametric Mann–Whitney test. *p < 0.05 was considered statistically

693 significant.

694 **Figure 3. *Pik3ca*-vascular malformations in murine retinas reproduce hallmarks of human**

695 **disease. (A)** Representative images of EC-*Pik3ca*[H1047R/WT] P6 retinas isolated from mice treated

696 with 0.125 mg/kg of 4-OHT on P1. Retinas were immunostained for blood vessels (IB4). Red

697 asterisks show arteries and arterioles and yellow arrowheads veins. Scale bars: 150 μm (left

698 panel) and 30 μm (right, high magnification panels). (**B**) Representative images of P6 retinas from

699 control and EC-*Pik3ca*[H1047R/WT] mice treated with 0.125 mg/kg 4-OHT on P1, following

28

700   immunostaining for p-S6 (S235/236) and blood vessels (IB4). Scale bars: 150 μm (left panels)

701   and 30 μm (right panels, high magnification). (**C**) Representative control and EC-*Pik3ca*[H1047R/WT]

702   P6 retinas immunostained for blood vessels (IB4), EC nuclei (Erg) and EdU. Scale bars: 150 μm

703   (left panels) and 30 μm (right panels, high magnification). Quantification of (**D**) p-S6 (S235/236)

704   intensity (presented as a fold change of vehicle-treated control), (**E**) EC proliferation by EdU

705   staining, (**F**) EC number by Erg positive cells and (**G**) retinal vascularity by IB4-positive area in

706   control and EC-*Pik3ca*[H1047R/WT] retinas. Error bars are s.e.m. n > 5 retinas per genotype. Statistical

707   analysis was performed by nonparametric Mann–Whitney test. **p < 0.01 was considered

708   statistically significant.

709   **Figure 4. Miransertib prevents the formation of *Pik3ca*-vascular malformations in mice.** (**A**)

710   4-OHT and miransertib dosing scheme used for a prevention therapeutic experimental setup. (**B,**

711   **C**) Representative images of P6 retinas isolated from control and EC-*Pik3ca*[H1047R/WT] mouse

712   littermates. Blood vessels were stained with IB4. Lower panels showing high magnification

713   images of the representative areas showing (**B**) blood vessels (IB4), EC nuclei (Erg), EdU

714   incorporation and (**C**) pS6 (S235/236). Quantification of (**D**) retinal vascularity by IB4 staining, (**E**)

715   EC number by Erg immunostaining, (**F**) EC proliferation by EdU staining, and (**G**) pS6 (S235/236)

716   intensity (presented as a fold change of vehicle-treated control). Scale bars: 150 μm (upper panel)

717   and 30 μm (lower panels). n ≥ 4 retinas per genotype. Statistical analysis was performed by

718   nonparametric Mann–Whitney test. *p < 0.05 and **p < 0.01 were considered statistically

719   significant.

720   **Figure 5. Low dose of miransertib prevents the growth of *Pik3ca*-vascular malformations.**

721   (**A**) 4-OHT and miransertib dosing scheme used for a prevention experimental setup. (**B, C**)

722   Representative confocal images of P6 retinas isolated from control and EC-*Pik3ca*[H1047R/WT] mouse

723   littermates. Blood vessels were stained with IB4. Lower panels showing high magnification

724   images of the representative areas showing (**B**) blood vessels (IB4), EC nuclei (Erg), EdU

725   incorporation and (**C**) pS6 (S235/236). Quantification of (**D**) retinal vascularity by IB4 staining, (**E**)

726   EC number by Erg immunostaining, (**F**) EC proliferation by EdU staining, and (**G**) pS6 (S235/236)

727   intensity (presented as a fold change of vehicle-treated control). Scale bars: 150 μm (upper

728   panels) and 30 μm (lower panels). n ≥ 3 retinas per genotype. Statistical analysis was performed

729   by nonparametric Mann–Whitney test. *$p < 0.05$ and **$p < 0.01$ were considered statistically

730   significant.

731   **Figure 6. Low dose miransertib induces regression of *Pik3ca*-vascular malformations *in***

732   ***vivo.*** (**A**) 4-OHT and miransertib dosing scheme used for a curative experimental setup. (**B, C**)

733   Representative confocal images of P6 retinas isolated from control and EC-*Pik3ca*[H1047R/WT] mouse

734   littermates. Blood vessels were stained with IB4. Lower panels showing high magnification

735   images of the representative areas showing (**B**) blood vessels (IB4), EC nuclei (Erg), EdU

736   incorporation and (**C**) pS6 (S235/236). Quantification of (**D**) retinal vascularity by IB4 staining, (**E**)

737   EC number by Erg immunostaining, (**F**) EC proliferation by EdU staining, and (**G**) pS6 (S235/236)

738   intensity (presented as a fold change of vehicle-treated control). Scale bars: 150 μm (upper

739   panels) and 30 μm (lower panels). n ≥ 4 retinas per genotype. Statistical analysis was performed

740   by nonparametric Mann–Whitney test. *$p < 0.05$ and **$p < 0.01$ were considered statistically

741   significant.

742   **Figure 7. Miransertib impairs cell viability of *PIK3CA*- and *TEK*-mutant patient-derived ECs.**

743   (**A**) Illustration showing the strategy of EC isolation from patient-derived biopsies. (**B**)

744   Representative sequencing chromatograms of *PIK3CA* and *TEK* mutant VM-derived ECs. Arrows

745   show the detected point mutations. (**C**) Representative confocal images of *PIK3CA* and *TEK*

746   patient-derived ECs immunostained for VE-cadherin (EC-specific junctional protein) and ERG

747   (EC-specific transcription factor). Cell nuclei were visualised with DAPI. Scale bars: 30 μm. (**D**)

748   Immunoblot showing the activation of PI3K/AKT/mTORC1 pathway (by assessing the levels of p-

749   AKT and p-S6) among different *PIK3CA* and *TEK* patient-derived ECs. Primary HUVEC were

750   used as wild type control. (**E-F**) Immunoblot showing the impact of miransertib at increasing doses

751   on PI3K/AKT/mTORC1 pathway (by assessing p-AKT and p-S6 levels) in (**E**) *PIK3CA* and (**F**)

752   *TEK* mutant patient-derived ECs. (**G**) *PIK3CA* and *TEK* mutant EC viability upon the treatment

753   with miransertib for 72h at different doses assessed by MTS assay. Fitting curves and 95% CI

754   IC50 values for both *PI3KCA* and *TEK* ECs are shown. Statistical analysis was performed by

755   comparison of best-fit values using the extra sum-of-squares F test.

30

Graphical abstract
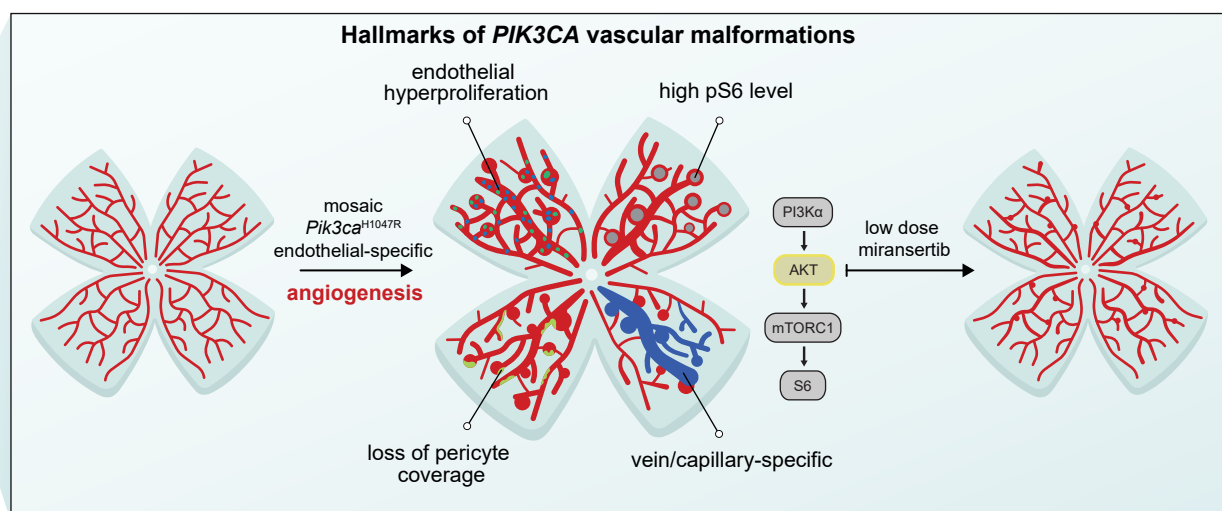
Low-flow vascular malformations are caused by PI3K signalling overactivation in endothelial cells. We have generated an optimised and robust preclinical system of PI3K-driven vascular malformations by inducing the mosaic expression of $Pik3ca^{H1047R}$ in the retinal angiogenic endothelium. This preclinical model displays traits constituting the main hallmarks of the pathogenesis of low-flow blood vascular malformations: overactivation of PI3K signalling (high phospho-S6), vascular compartment specificity, loss of pericyte coverage, and endothelial cell hyperproliferation. Using this preclinical model we report that low dose AKT inhibitor miransertib prevents and regress PI3K-driven vascular malformations.

Figure 1

A

angiogenesis stage:

early

intermediate

late

▼ 25 mg/kg 4-OHT
▼ retina isolation

P1 ... P6
P7 ... P15
P15 ... P21

B

C

P1 → P6   P6 → P15   P15 → P21

■ generalised VM
■ focal VM
■ no VM

16/16   16/16   16/48

D

E

F

Figure 2

Figure 3

Figure 4

A

▼ 0.125 mg/kg 4-OHT
🖉 75 mg/kg miransertib/vehicle
▼ retina isolation

P1 P2   P6

B

control — vehicle | miransertib
EC-$Pik3ca^{H1047R/WT}$ — vehicle | miransertib

IB4
IB4
Erg:EdU

C

control — vehicle | miransertib
EC-$Pik3ca^{H1047R/WT}$ — vehicle | miransertib

IB4:pS6
pS6

D

% IB4$^+$ per 10^4 μm^2

* p = 0.016
** p = 0.009

miransertib − +   − +
control | EC-$Pik3ca^{H1047R/WT}$

E

EC no. per 10^4 μm^2

* p = 0.016
** p = 0.009

miransertib − +   − +
control | EC-$Pik3ca^{H1047R/WT}$

F

EdU$^+$ EC per 10^4 μm^2

* p = 0.016
** p = 0.005

miransertib − +   − +
control | EC-$Pik3ca^{H1047R/WT}$

G

pS6 intensity (fold change)

* p = 0.019
* p = 0.041

miransertib − +   − +
control | EC-$Pik3ca^{H1047R/WT}$

Figure 5

Figure 6

Figure 7